Landsat-7 ETM+ Radiometric Calibration Status

Julia A. Barsi *[a], Brian L. Markham [b], Jeffrey S. Czapla-Myers [c],
Dennis L. Helder [d], Simon J. Hook [e], John R. Schott [f], Md. Obaidul Haque [g]
[a] SSAI, NASA/GSFC, Greenbelt MD USA 20771; [b] NASA/GSFC, Greenbelt MD 20771;
[c] University of Arizona, Tucson AZ 85721 USA; [d] South Dakota State University, Brookings SD 57007 USA; [e] NASA/JPL, Pasadena CA 91109; [f] Rochester Institute of Technology, Rochester NY 14623; [g] SGT, USGS/EROS, Sioux Falls, SD 57198

ABSTRACT

Now in its 17th year of operation, the Enhanced Thematic Mapper + (ETM+), on board the Landsat-7 satellite, continues to systematically acquire imagery of the Earth to add to the 40+ year archive of Landsat data. Characterization of the ETM+ on-orbit radiometric performance has been on-going since its launch in 1999. The radiometric calibration of the reflective bands is still monitored using on-board calibration devices, though the Pseudo-Invariant Calibration Sites (PICS) method has proven to be an effect tool as well. The calibration gains were updated in April 2013 based primarily on PICS results, which corrected for a change of as much as -0.2%/year degradation in the worst case bands. A new comparison with the SADE database of PICS results indicates no additional degradation in the updated calibration. PICS data are still being tracked though the recent trends are not well understood.

The thermal band calibration was updated last in October 2013 based on a continued calibration effort by NASA/Jet Propulsion Lab and Rochester Institute of Technology. The update accounted for a 0.31 W/m^2 sr μm bias error. The updated lifetime trend is now stable to within +/- 0.4K.

Keywords: Landsat, ETM+, radiometry, calibration, reflective, thermal

1. INTRODUCTION

The Landsat-7 Enhanced Thematic Mapper+ (ETM+) has continued the long history of Earth observing from space by the Landsat project. The ETM+ is a whiskbroom sensor with a 16-day repeat cycle. The failure of the Scan Line Corrector (SLC) in 2003 left the imager with gaps in its coverage, but the image data that are acquired have been very high quality for the entire lifetime. Basic characteristics of the ETM+ are listed in Table 1.

The calibration is an important part of maintaining the quality of the archive. The radiometric calibration has comprehensively been written about in [1] and [2] for the reflective bands and [3] and [4] for the thermal bands. The purpose of this paper is to update the status of the radiometric calibration of the ETM+ since the previous papers.

Table 1. ETM+ basic characteristics.

Band	Band "color"	Bandpass (nm)	IFOV (m)	Number of Detectors
1	Blue	441-514	30	16
2	Green	519-601	30	16
3	Red	631-692	30	16
4	NIR	772-898	30	16
5	SWIR-1	1547-1748	30	16
6	thermal	10.31-12.36 μm	60	8
7	SWIR-2	2065-2346	30	16
8	Pan	515-896	15	32

julia.barsi@nasa.gov; phone 1 301 614-6667; fax 1 301 614 6695

2. REFLECTIVE BANDS

The reflective band radiometry has been written about in [1] and [2]. The intent of this paper is to update the status of the radiometric characterization and calibration from the 2012 paper. The aspects that have not changed will not be covered; those include the total noise, the bias levels and the relative gains. There have been changes in the nature of the coherent noise in the ETM+ Band 5. Also, since the 2012 paper, long-term trending indicated the need for a change to the absolute radiometric calibration. All the data in this paper have been reprocessed with the 2013 calibration update though due to the organization of the paper, the gain change will be discussed in the Pseudo-Invariant Calibration Sites (PICS) section, not at the beginning of the section.

2.1 Coherent Noise

Coherent noise in the ETM+ has been monitored since launch with little change in the primary frequencies. A fast Fourier transform is performed on dark nighttime data. Figure 1 shows the power history of the coherent noise features detected by frequency analysis. The Band 5 noise affects two detectors: detectors 10 and 12. It was originally identified at 20 kHz though over time the peak frequency has shifted to 18 kHz. The power of the noise has also changed. Starting in about 2007, the power began increasing and it has not stopped. The power and frequency are highly correlated with instrument on-line; the noise diminishes as the instrument remains on. In 2010, only the first few scenes acquired in an interval (after the ETM+ had been powered off) were affected by the coherent noise. At the beginning of the interval, the peak-to-peak noise was 1.5 DN and 7 minutes later the noise was not visible. However, by 2015 the noise is strong enough that it is still present at the end of intervals, up to 15 minutes later. One sample interval started with 6 DN peak-to-peak noise and by 11 minutes later, the noise had reduced to 2-3 DN peak-to-peak. Figure 2 shows a sample of the coherent noise in an image acquired about 1 minute after the ETM+ was turned on. The magnitude of the coherent noise is about 6 counts and is clearly visible in the image.

There is no correction implemented in the processing system to account for the Band 5 coherent noise as of yet.

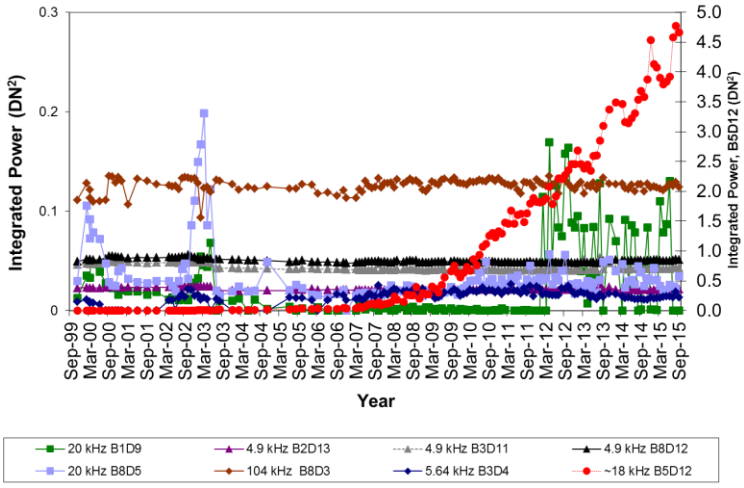

Figure 1. Sample coherent noise features in the ETM+ as detected by Fourier analysis of nighttime dark images. A representative detector of each band for each frequency is shown. The y-axis scale on the right hand side is for the B5 18kHz noise source only. Although detectable in frequency analysis, the coherent noise is generally not visible in imagery, except for the B5 noise in the recent years, which is likely visible in most images dependent on scene content.

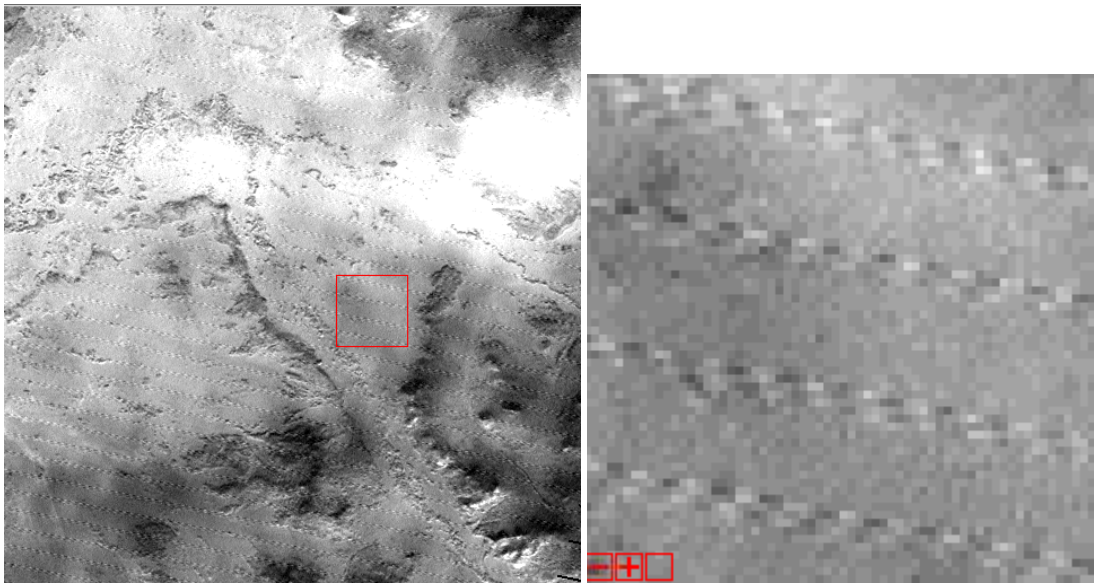

Figure 2. Sample image illustrating the Band 5 coherent noise; 21 Nov 2015, 128/23, ETM+ was on for ~1 minute. The peak-to-peak noise is ~6 DN. The image on the right is a subset of the image on the left. These are samples from a geometrically resampled image, so the per-detector coherent noise is averaged via cubic convolution with the neighboring detectors.

Table 2. ETM+ reflective band operational calibration methods.

Calibrator	Frequency	Precision
Internal Calibrator (IC) lamp and shutter system	per-scan	tenths of percent
Full Aperture Solar Panel (FASC) diffuser panel	monthly	tenths of percent
Vicarious Calibration (on-site personnel)	4-6 per site per year (travel, weather dependent)	2.5-7%
Vicarious Calibration (automated)	up to 16 per year (weather, instrumentation dependent)	4%
Pseudo-Invariant Calibration Sites (PICS)	up to 16 per year per site (weather dependent)	~1-2%

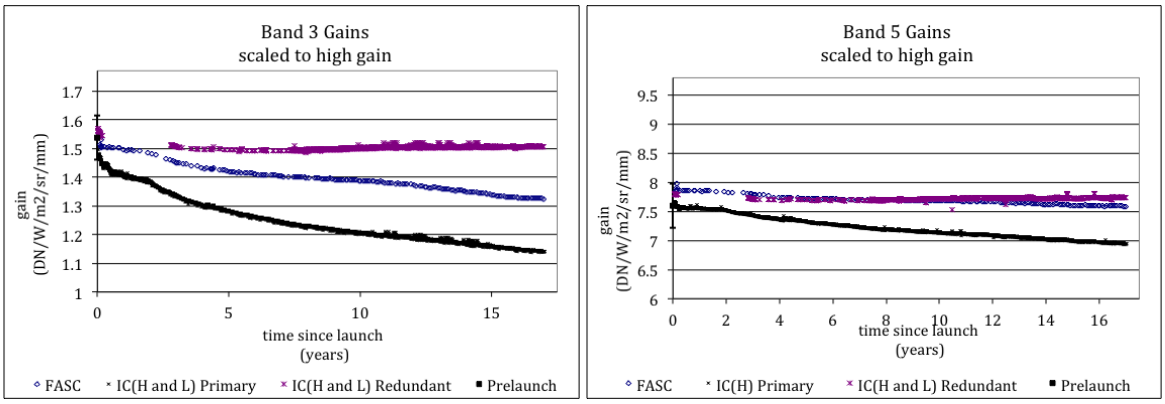

Figure 3. The ETM+ response to the operational on-board calibrators for Bands 3 and 5. The prelaunch gain is also shown at year 0 along with +/-5% error bars.

2.2 On-Board Calibrators

The on-board calibrators still in use on the ETM+ are the Internal Calibrator (IC) lamp system and the Full Aperture Solar Calibrator (FASC) diffuser panel. There are two lamps in the IC which are used at different frequencies: the redundant lamp is two orbits out of a 16 day cycle and the primary lamp is used for the rest of the orbits. The FASC panel is used monthly. Table 2 lays out the calibrators in use for the reflective bands of the ETM+ and their precision.

The primary lamp has been particularly unstable, changing more than 1% per year in most bands. The redundant lamp and the FASC have been better behaved but the ETM+ appears to be tracking instability in them rather than the calibrators providing a measure of the ETM+ instability. The ETM+ response to the primary and redundant lamps and the FASC are shown in Figure 3 for sample Bands 3 and 5. The other bands display similar levels of instability.

2.3 Vicarious Calibration

The University of Arizona (UofA) and South Dakota State University (SDSU) both acquire vicarious calibration data under the ETM+ [5]. The UofA has traditionally attempted field campaigns 4-6 times per year at Railroad Valley and Ivanpah Playa, but success was dependent on the weather. SDSU takes measurements on a large grass field near Brookings, SD. With the addition of an automated measurement system, Radiometric Calibration Test Site (RadCaTS) [6], more regular validation data should become available. Between February 2012 and May 2016, there were 25 successful RadCaTS measurements for ETM+.

All data presented here were reprocessed with the latest version of the calibration gains. There are fewer UofA points here than in previous versions of these plots as the UofA processing system has also advanced and in some cases, the UofA the historical data was in the wrong format or was lost so could not be reprocessed. Not all RadCaTS data were available at the time of this writing and the SDSU dataset has not been updated to include the latest calibration update. The valid per-acquisition data are shown in Figure 4 for two sample bands. The UofA on-site personnel data are reduced to lifetime average differences with the ETM+ in Figure 5.

The vicarious calibration results continue to show sufficient scatter that it is difficult to discern real trends in the ETM+ response.

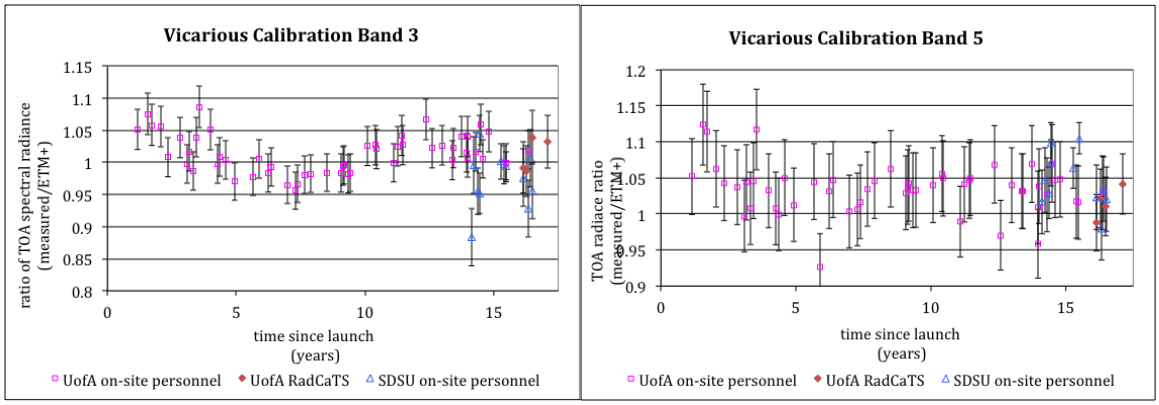

Figure 4. The ratio between the surface-measurement predicted TOA reflectance to the ETM+ measured TOA reflectance for two sample bands. There are only a few RadCaTS and SDSU data points included here due to uncertainty in the processing pedigree. The on-site personnel data series include error bars of 3% in Band 3 and 5% in Band 5. The RadCaTS data include 4% error bars. The SDSU error bars are based on individual assessments of the quality of the atmospheric correction on the specific date.

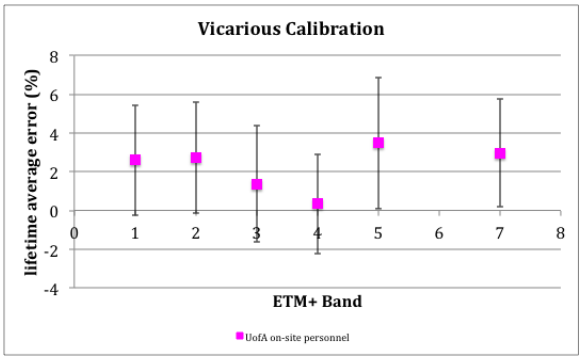

Figure 5. Average calibration error as estimated from the UofA on-site personnel data. SDSU and RadCaTS averages are not included here as not enough data has been reprocessed to estimate a lifetime average.

2.4 Pseudo-Invariant Calibration Sites

The Pseudo-Invariant Calibration Sites (PICS) typically used by Landsat are a subset from those defined by [7], referred to here as the CNES regions, and currently used by many satellite programs to monitor stability. The sites used by the Landsat program for continuous monitoring are shown in Table 3, listing both the CNES region name and the Landsat WRS-2 path/row frame. The CNES regions were defined to be about 20x20km and all are not necessarily situated completely within a single WRS-2 frame. As a result, the Landsat team picked a more convenient, larger region to track, a 90km box around the nominal scene center of the WRS-2 frame. Advances in the processing system have recently made it easier to track multiple regions, so work has started to monitor the CNES region as well, where possible. To date, eight of the 20 CNES sites have been fully trended by the Landsat processing system. A review of the regions that have both small and large regions defined has shown that there is not a statistically significant difference between the CNES 20x20km region and the Landsat 90x90km region (Table 4 and Figure 6). The region-average reflectances are within 0.5% (1-sigma) across all bands and the lifetime-trended slopes are indistinguishable.

2.4.1 Long-Term Trending

For long-term trending, standard Level-1 processed images are used. The region-average top-of-atmosphere (TOA) radiance is converted to TOA reflectance using the E_{sun} provided with the image product. An empirical linear correction

for solar elevation angle is applied to remove some of the seasonality from the trends. The reflectances are normalized and the slope of the trend is determined via linear regression. The slope is the indicator of long-term degradation.

In 2012, the slopes of the lifetime trends were statistically significant [8] and by 2013, the affect was as large as 2.8% in the worst bands [9]. The calibration gains were updated for all bands based on a weighted average of the four individual PICS sites being tracked at the time (Table 3). The whole ETM+ archive was eventually reprocessed with the new gains, including all the PICS sites. A new analysis of the lifetime trend indicates that for the lifetime, there is no residual error (Figure 7). For analysis of the data acquired since the update (2013-2016), the picture is less certain. There are indications that the degradation may have increased in some bands though not across all bands. The assessment is less clear when individual sites are considered and when comparing trends between instruments. This is an active area of study and no additional actions will be taken to correct the ETM+ until the data are better understood.

Table 3. The PICS sites tracked by ETM+ for long-term stability monitoring. Every opportunity to image these sites has been acquired since ~2003. The asterisk (*) indicates the site was being monitored in 2012 and was used for the 2012 calibration gain update. The other sites are monitored regularly now.

Site	Landsat Path/Row	Number of Clear Acquisitions as of 2016
Libya-4*	181/40	160
Sudan-1*	177/45	182
Mauritania-2*	201/46	62
Arabia-1*	165/47	119
Algeria-3	192/39	122
Libya-1	187/43	139

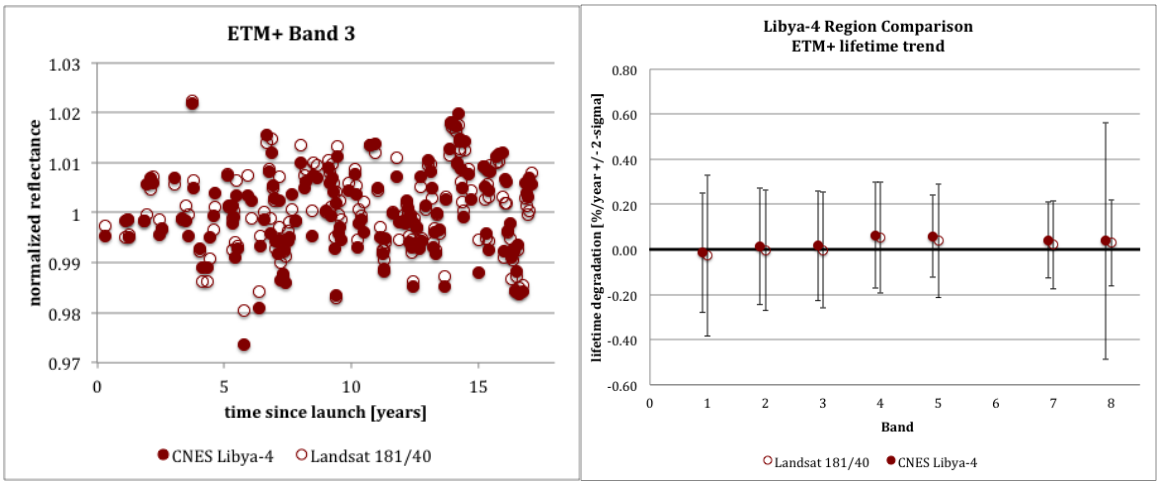

Figure 6. Comparison of lifetime trends of the 20x20km CNES Libya-4 region and the 90x90km Landsat 181/40 region. The left plot shows the region-average reflectance in Band 3 for every clear acquisition of 181/40 for both regions. The right plot shows the slope of the lifetime trend for both regions, along with 2-sigma error bars. The data sets are statistically identical for the purposes of long-term trending.

Table 4. Average differences between the CNES Libya-4 region and the Landsat 181/40 region for the lifetime of ETM+. The dataset includes 160 acquisitions of the site. The calculation is (CNES-ETM+)/ETM+ in TOA reflectance.

Band	Average Reflectance Difference (%)	Standard Deviation (%)
1	-0.01	0.40
2	-0.02	0.31
3	-0.03	0.26
4	0.01	0.35
5	-0.03	0.28
7	-0.03	0.42

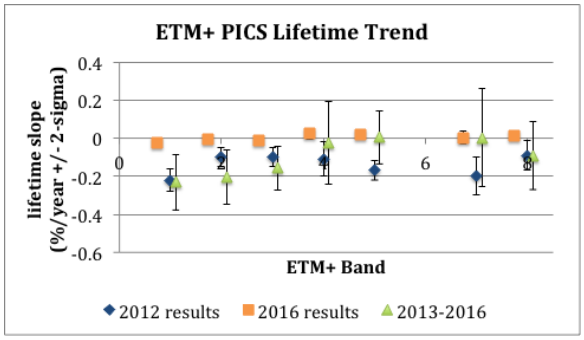

Figure 7. The lifetime weighted average slope of the monitored PICS sites in 2012 and 2016 as well as the trend for just the last 3 years of data. The 2013 calibration update was based on the results from 2012 and the 2016 analysis using data processed with the calibration update shows no residual degradation in the calibration over the lifetime. Considering just the last three years, however, the PICS sites are indicating some additional degradation that is not fully understood yet.

2.4.2 SADE Analysis

CNES has built a multi-satellite database of reflectances from the CNES sites called SADE and developed an algorithm to cross-calibrate pairs of instruments [10]. The database includes data from at least 20 different instruments. In 2016, Landsat-7 ETM+ data for 8 of the CNES 20x20km sites were added to the SADE database and the first cross-calibration between ETM+ and other available sensors were run. ETM+ was compared to Aqua MODIS, MERIS, Landsat-8 OLI and Sentinel-2 MSI. Due to the very short lifetimes of OLI and MSI, only the MODIS and MERIS comparisons will be shown here.

The CNES analysis concludes that there is no significant residual drift in calibration over 17 years and the ETM+ is within 2% of the other instruments for Bands 1, 2, 3, and 4. The larger difference in Band 5 is likely due to lack of good spectral match with the reference instruments: the ETM+ SWIR-1 band is much wider than the MODIS band in that wavelength region. Neither MODIS nor MERIS has a band equivalent to SWIR-2 so there is no comparison for Band 7. Figure 7 shows the cross-calibration results with Aqua MODIS for the VNIR bands. Table 5 details average differences between the MODIS and MERIS reflectances and the ETM+ reflectances.

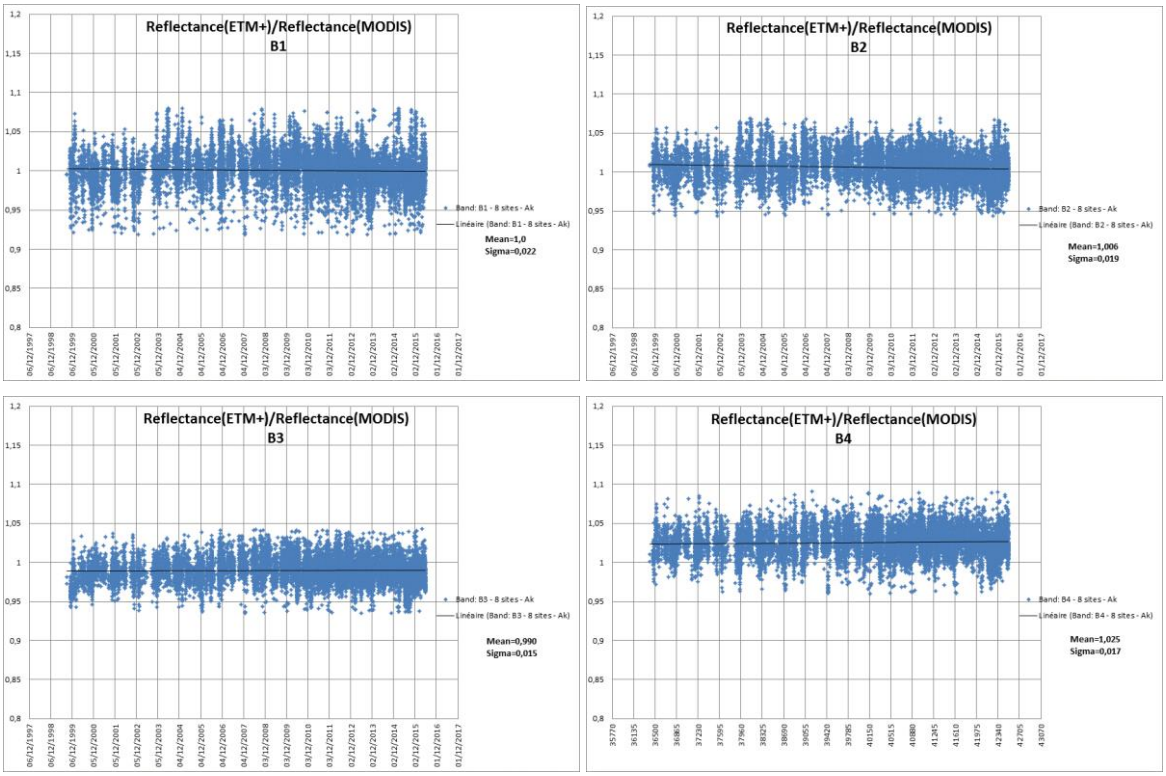

Figure 8. The CNES SADE cross-calibration of ETM+ and Aqua MODIS for each of the ETM+ VNIR bands. The data don't indicate any residual drift in the ETM+ calibration as compared to MODIS. Analysis and plots courtesy of CNES.

Table 5. Average differences between the ETM+ and reference instrument based on the SADE cross-calibration analysis. The larger difference between ETM+ and MODIS in the SWIR-1 is likely due to the difference in the bandpass widths. Neither MODIS nor MERIS have an equivalent SWIR-2 band to which to compare.

Band	ETM+/Aqua MODIS ratio	ETM+/MERIS ratio	Average Difference (%)
1	1.000	0.997	-0.15
2	1.006	0.978	-0.8
3	0.990	0.986	-1.2
4	1.025	1.009	1.7
5	0.962	N/A	-3.8
7	N/A	N/A	N/A

2.5 Reflectance Calibration Update

The reflectance calibration of the ETM+ is currently based on the Chance-Kurucz solar spectra (ChKur); the solar irradiance (E_{sun}) provided in the metadata files is the integration of Chance-Kurucz over the ETM+ bandpasses. To be more consistent with the OLI, work has been done to estimate a new E_{sun} that is tied to the to the OLI reflectance calibration rather than a solar model [11]. The new "E_{sun}" values will be replacing the Chance-Kurucz E_{sun} in the image

product metadata by the end of 2016, coming with the implementation of Collections processing [12]. The new E_{sun} will change the estimated reflectance in every band (Table 6). See [11] for more details.

This change will affect the CNES SADE cross-calibration results but not the PICS lifetime trending or the vicarious calibration results. The SADE analysis is affected because it compares ETM+ reflectances to the reference instruments. The PICS trending is not affected because it is based on the overall slope and the change in bias won't make a difference. Vicarious calibration is dependent on the radiance calibration which is independent of this change.

Table 6. ETM+ reflectance calibration change per-band as estimated by the difference in solar irradiance values.

Landsat 7 ETM+				
Band	Reflectan-ce Gain	ESUN (L8)	ESUN (ChKur)	%Diff
1	529.02	2036	1970	-3.24
2	468.93	1856	1842	-0.75
3	497.36	1525	1547	1.44
4	339.86	1071	1044	-2.52
5	356.88	221.6	225.7	1.85
7	376.37	81.36	82.06	0.86
8	415.13	1319	1369	3.79

3. THERMAL BAND

The latest paper on the state of the ETM+ thermal band was in 2012 [13]. Since that publication, an update to the ETM+ thermal band calibration was made based on the vicarious calibration data [9]. The overall health of the thermal band remains stable: no changes in noise levels, bias levels, or relative gains. This section will only cover the most recent vicarious calibration results.

3.1 On-board calibrator

The ETM+ thermal band on-board calibration system consists of a thermally controlled blackbody and a shutter at ambient for a two-point linear calibration. The ETM+ sees the blackbody and the shutter every scan. The calibration gain and offset determined from this system have been incredibly stable over the lifetime, only changing when updates to the calibration are made to account for errors in calibration as determined by the vicarious calibration results.

The gain has been stable to within 0.04%/year since 2013 and the bias to within 0.03%/year since 2013 (Figure 10).

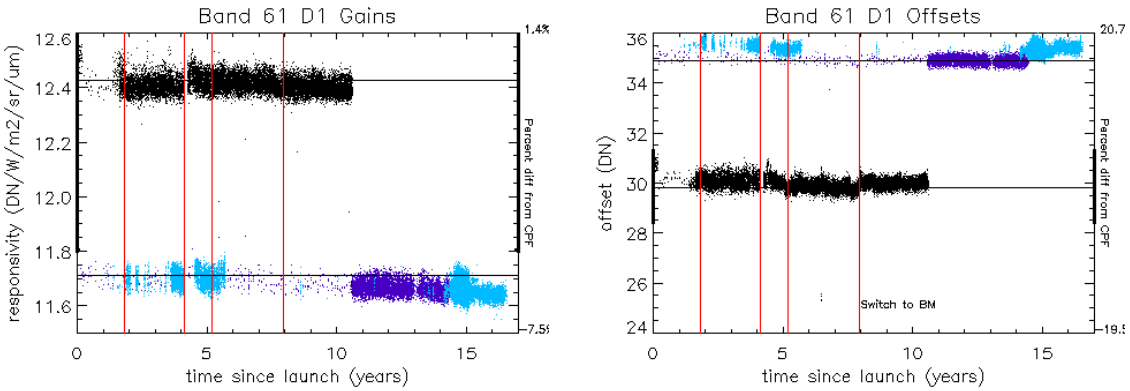

Figure 9. Lifetime trends of the ETM+ thermal band responsivity and offset as calculated from the on-board calibration system. The large changes in gain and offset are the result of changes to the calibration coefficients, not due to changes in the instrument. The data plotted in light blue are the data processed with the current calibration parameters.

3.2 Vicarious Calibration

The vicarious calibration of the thermal band is based on radiance or temperature measurements of large water bodies which are converted to a TOA radiance for comparison to the satellite measurement. Teams at NASA/JPL operates radiometric calibration buoys on Lake Tahoe and the Salton Sea [14]; the Rochester Institute of Technology mines the NOAA National Buoy Data Center for buoys with appropriate characteristics for vicarious calibration [13]. The surface measurement is corrected for a skin temperature effect if needed, projected through the atmosphere using MODTRAN and compared to the satellite-measured radiance.

In 2013, the teams detected a 0.036 W/m^2 sr μm bias error in the data. The error was corrected in the processing system in Oct 2013 [9]. The data acquired since then have been stable to within 0.06 W/m^2 sr μm or 0.4K at 300K (Figure 11, Table 7).

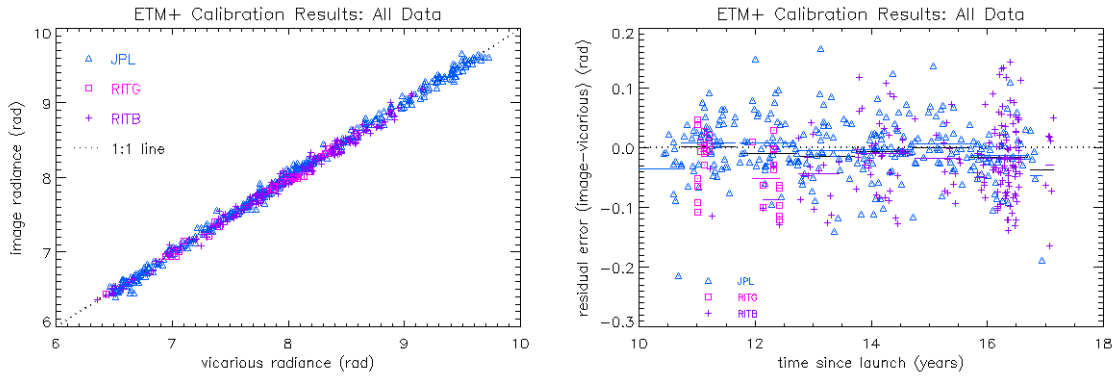

Figure 10. Vicarious calibration data since 2009. All data have been reprocessed with the latest calibration update. On the left, the plot shows all the data fall on the 1:1 line. On the right, the plot shows that the residual errors are random about 0.0.

Table 7. Vicarious calibration regression results for the RIT and JPL data sets combined. The lifetime slope and bias are not significant with an uncertainty of less than 0.5K.

Team	N	Regression slope +/- 95% CI [W/m^2 sr μm /year]	Residual bias +/- 95% CI [W/m^2 sr μm]	RMSE [W/m^2 sr μm]	RMSE [K at 300K]
all data	597	1.00 ± 0.01	-0.01 ± 0.00	0.06	0.4

4. SUMMARY AND CONCLUSIONS

The ETM+ is in its seventeenth year of operations and continues to provide valuable science data to the community. The 18 kHz coherent noise feature in Band 5 Detectors 10 and 12 has grown in power and is now likely visible in most imagery (dependent on scene content). There is currently no correction in place for this. The ETM+ itself is more stable than the on-board calibration systems. Monitoring the calibration with PICS has proven to be an important tool; the gains were updated in 2013 based on long-term degradation detected using the PICS dataset. Since the calibration update, the PICS continue to be monitored though recent trends are still not fully understood. Analysis from the CNES SADE database comparing ETM+ to MODIS and MERIS through PICS reveals good consistency between the instruments, less than 2% difference in the VNIR bands, and no long-term residual drift.

The thermal band on-board calibration system has remained stable since launch with far less than 0.1% change per year detected. The vicarious calibration sources detected a small bias error of 0.036 W/m^2 sr μm in 2012. That was corrected in the processing system in Oct 2013 and since then, there has been no additional detectable error; the thermal band is stable to 0.06 W/m^2 sr μm or 0.4K at 300K.

ACKNOWLEDGEMENT

Thank you to A. Meygret, B. Besson and C. Miquel of CNES for getting the ETM+ and OLI PICS data into the SADE database and running the cross-calibration assessment.

REFERENCES

[1] P. L. Scaramuzza, B. L. Markham, J. A. Barsi, and E. Kaita, "Landsat-7 ETM+ on-orbit reflective-band radiometric characterization," *IEEE Trans. Geosci. Remote Sens.*, vol. 42, no. 12, pp. 2796–2809, Dec. 2004.

[2] Markham, B.L.; Haque, M.O.; Barsi, J.A.; Micijevic, E.; Helder, D.L.; Thome, K.J.; Aaron, D.; Czapla-Myers, J.S., "Landsat-7 ETM+: 12 Years On-Orbit Reflective-Band Radiometric Performance," in Geoscience and Remote Sensing, IEEE Transactions on, vol.50, no.5, pp.2056-2062, May 2012

[3] Barsi, J.A, Schott, J.R., Palluconi, F.D., Helder, D.L., Hook, S.J., Markham, B.L., Chander, G., O'Donnell, E.M. (2003). Landsat TM and ETM+ Thermal Band Calibration. Canadian Journal of Remote Sensing, Vol. 29, No. 2.

[4] John R. Schott, Simon J. Hook, Julia A. Barsi, Brian L. Markham, Jonathan Miller, Francis P. Padula, Nina G. Raqueno, "Thermal Infrared Radiometric Calibration of the Entire Landsat 4, 5, and 7 Archive (1982-2010)." Remote Sensing of Environment, July 2012.

[5] K. J. Thome, D. L. Helder, D. Aaron and J. D. Dewald, "Landsat-5 TM and Landsat-7 ETM+ absolute radiometric calibration using the reflectance-based method," in *IEEE Transactions on Geoscience and Remote Sensing*, vol. 42, no. 12, pp. 2777-2785, Dec. 2004.

[6] Czapla-Myers, J.; McCorkel, J.; Anderson, N.; Thome, K.; Biggar, S.; Helder, D.; Aaron, D.; Leigh, L.; Mishra, N. The Ground-Based Absolute Radiometric Calibration of Landsat 8 OLI. *Remote Sens.* **2015**, *7*, 600-626.

[7] H. Cosnefroy, M. Leroy, and X. Briottet, "Selection and characterization of Saharan and Arabian desert sites for the calibration of optical satellite sensors," *Remote Sens. Environ.*, vol. 58, no. 1, pp. 101–114, Oct. 1996.

[8] J. A. Barsi, B. L. Markham and D. L. Helder, "Continued monitoring of Landsat reflective band calibration using pseudo-invariant calibration sites," *2012 IEEE International Geoscience and Remote Sensing Symposium*, Munich, 2012, pp. 7007-7010.
[9] ----, "Landsat 7 (L7) Enhanced Thematic Mapper Plus (ETM+) Calibration Notices," USGS, 29 Oct 2015, http://landsat.usgs.gov//science_L7_Cal_Notices.php (30 Aug 2016)
[10] S. Lacherade, B. Fougnie, P. Henry and P. Gamet, "Cross Calibration Over Desert Sites: Description, Methodology, and Operational Implementation," in *IEEE Transactions on Geoscience and Remote Sensing*, vol. 51, no. 3, pp. 1098-1113, March 2013. doi: 10.1109/TGRS.2012.2227061
[11] Micijevic, E.; Haque, M.O.; Mishra, N., Radiometric calibration updates to the Landsat collection. Proc. SPIE 9972, Earth Observing Systems XXI (2016)
[12] Morfitt, R. Proc. SPIE 9972, Earth Observing Systems XXI (2016)
[13] John R. Schott, Simon J. Hook, Julia A. Barsi, Brian L. Markham, Jonathan Miller, Francis P. Padula, Nina G. Raqueno, Thermal infrared radiometric calibration of the entire Landsat 4, 5, and 7 archive (1982–2010), Remote Sensing of Environment, Volume 122, July 2012, Pages 41-49, ISSN 0034-4257, http://dx.doi.org/10.1016/j.rse.2011.07.022.
[14] Hook, S.J.; Vaughan, R.G.; Tonooka, H.; Schladow, S.G. Absolute radiometric in-flight validation of mid infrared and thermal infrared data from ASTER and MODIS on the Terra spacecraft using the Lake Tahoe, CA/NV, USA, automated validation site. *IEEE Trans. Geosci. Remote Sens.* **2007**, *45*, 1798–1807.